Sustainable Cities and Society 69 (2021) 102818

Contents lists available at ScienceDirect

Sustainable Cities and Society

journal homepage: www.elsevier.com/locate/scs

Understanding land surface temperature impact factors based on local climate zones

Jun Yang [a,b,*], Jiayi Ren [a], Dongqi Sun [c,**], Xiangming Xiao [d], Jianhong (Cecilia) Xia [e], Cui Jin [a], Xueming Li [a]

[a] Human Settlements Research Center, Liaoning Normal University, Dalian, 116029, China
[b] Jangho Architecture College, Northeastern University, Shenyang, 110169, China
[c] Key Laboratory of Regional Sustainable Development Modeling, Institute of Geographic Sciences and Natural Resources Research, CAS, Beijing, 100101, China
[d] Department of Microbiology and Plant Biology, Center for Spatial Analysis, University of Oklahoma, Norman, OK, 73019, USA
[e] School of Earth and Planetary Sciences (EPS), Curtin University, Perth, 65630, Australia

ARTICLE INFO

Keywords:
Urban thermal environment
Local climate zone (LCZ)
Building structure parameters
Remote sensing index
Shenyang

ABSTRACT

The local climate zone (LCZ) and land surface temperature (LST) have gained considerable attention as urbanization continues to increase. However, the study of LSTs lacks a regional complexity perspective. In order to explore the law of urban thermal environment, impact factors of LSTs are identified using GIS spatial analysis and statistical analysis methods in conjunction with parameter models that reflect urban spatial morphologies on the LCZ scale. The research results show that the LST ranges from 24.90 °C (LCZA) to 33.26 °C (LCZ2) in the summer of 2017 and from 2.53 °C (LCZ7) to 2.89 °C (LCZ3) in winter; LST ranged from 22.00 °C (LCZ2) to 28.19 °C (LCZE) in summer 2019, and from -4.79 °C (LCZ10) to -2.12 °C (LCZ3) in winter. Different LCZs had different impacts on LSTs. LST is always positively correlated with the floor area ratio, with a maximum correlation coefficient of 0.682 in LCZ2. It exhibits the highest positive correlation (correlation coefficient = 0.421) with average building height in LCZ3 and the highest negative correlation (correlation coefficient = -0.706) in LCZ7; vegetation and water bodies have a cooling effect. These results can serve as a valuable reference for building cool communities and improving the living environment of residents.

1. Introduction

From the end of the 20th century to the 21st century, the most significant change to the human environment has been the rapid development of cities worldwide. Widespread construction of impervious materials and buildings has altered the characteristics of the original land surface and has become increasingly more complex, leading to climate change and a series of environmental problems (He, 2018; Panagopoulos, Gonzalez Duque, & Bostenaru Dan, 2016; Qiao et al., 2019; You et al., 2021). Particularly, in metropolitan areas with developed industries and rapid economic growth, where populations are concentrated and waste is discharged into the surrounding air, soil, or water, the local thermal environment and microclimate have changed to varying degrees (Yang, Ruby Leung et al., 2017; He, Wang, Liu, & Ulpiani, 2019). This has disrupted the energy balance, resulting in urban heat island (UHI) effects that directly/indirectly affect the health and living standards of residents (Budhiraja, Gawuc, & Agrawal, 2019; Emmanuel & Krüger, 2012). The UHI concept reflects the overall microclimate changes caused by urbanization, where the land surface temperature (LST) indicates the degree of land surface warming (Tv, Aithal, & Sanna, 2012; Yang, Yang et al., 2019). Therefore, reducing the rise in LST to prevent further aggravation of urban thermal environment problems has attracted increasing research interest.

Understanding the factors driving urban LST is a prerequisite for its effective control (Wang & Ouyang, 2017). Previous studies have researched the effects of land use/land cover, landscape patterns, human activity, meteorological conditions, geographical locations, and other aspects (Bartesaghi Koc, Osmond, Peters, & Irger, 2018; Guo, Yang, Sun et al., 2020; Kong et al., 2017; Yang, Wang et al., 2019). The urban LST is closely related to land surface attributes, and the average LST is

* Corresponding author at: Human Settlements Research Center, Liaoning Normal University, Dalian, 116029, China.
** Corresponding author.
E-mail addresses: yangjun8@mail.neu.edu.cn (J. Yang), renjiayi_gis@163.com (J. Ren), sundq@igsnrr.ac.cn (D. Sun), xiangming.xiao@ou.edu (X. Xiao), c.xia@curtin.edu.au (J.(C. Xia), cuijin@lnnu.edu.cn (C. Jin), lixueming999@163.com (X. Li).

https://doi.org/10.1016/j.scs.2021.102818
Received 4 November 2020; Received in revised form 21 February 2021; Accepted 26 February 2021
Available online 1 March 2021
2210-6707/

significantly correlated with the impervious surface density (positive) and vegetation coverage (negative) (Amiri, Weng, Alimohammadi, & Alavipanah, 2009; Estoque, Murayama, & Myint, 2017; Song, Du, Feng, & Guo, 2014). The spatial distribution and structure of the impervious surface (such as patch size and shape) have different effects on LST; the higher the spatial concentration, the higher the LST (Gulbe, Caune, & Korats, 2017; Zhou, Wang, & Cadenasso, 2017). Also, the horizontal and vertical distribution of buildings are nonuniform, narrow streets and tall buildings block heat and ventilation, and wide urban vision facilitate air circulation and heat dissipation (Yang, Wang et al., 2019). In order to accurately describe the impact of different forms of buildings on LST, it is meaningful to construct and calculate the indicators of building form (Bernard, Bocher, Petit, & Palominos, 2018; Bernard, Bocher, Petit, & Palominos, 2018; He, Ding, & Prasad, 2019). To enhance the livability of cities, cool cities and cool communities should be promoted, which should include the construction of cool roofs/sidewalks/walls and urban vegetation (Gilbert, Mandel, & Levinson, 2016). However, for developing countries, especially densely populated areas, there is no longer a clear dividing line between social, political, and economic spaces. Moreover, with the migration of populations or economic centers, old cities are shrinking while emerging development zones are expanding (Chen et al., 2019; Li, Yan, Bian, Liu, & Wu, 2020; Ma et al., 2015). This study considers that for some densely populated areas with diversified land use patterns, the study of LST influencing factors cannot be carried out only on a single scale (Portela, Massi, Rodrigues, & Alcântara, 2020; Xie, Yang, Wang, Liu, & Liu, 2020; Yang, Luo, Jin, Xiao, & Xia, 2020).

To comprehensively consider the impacts of urban morphology on LST, Stewart and Oke used the urban boundary layer to define the urban canopy layer as the atmospheric layer extending from the roof of the building to the ground (Oke, 1973; Stewart & Oke, 2012). This research also divided the city into 17 climate zones; that is, local climate zones (LCZs) that represent a simple combination of surface features, which has provided new insights for urban thermal environment research. Previous studies demonstrate that the LST of an LCZ is closely related to factors such as geographic location, city size, water permeability, building height and spacing and vegetation density, (Bechtel et al., 2015; Thomas, Sherin, Ansar, & Zachariah, 2014; Unger, Lelovics, & Gál, 2014; Zhao, Ma, Zhong, Zhao, & Cao, 2019; Zheng et al., 2018). An analysis of spatiotemporal variations of LST based on LCZ clearly showed that temperature varies among different LCZs (Hu et al., 2019). The LST of a building-type LCZ is higher than that of a natural-type LCZ (Shi, Lau, Ren, & Ng, 2018; Yang, Zhan et al., 2020). Among natural-types, the bare-land LSTs are relatively higher, whereas those of water bodies and forests are relatively lower (Krayenhoff & Voogt, 2016; Ochola et al., 2020). Moreover, on the micro scale, it was found that wind can reduce the LST, though the efficacy and effect of the wind varies between LCZs according to building-type and surface (Yang, Jin et al., 2019). Therefore, lands surface geometry is an important factor affecting the distribution of LST within cities (Gál, Lindberg, & Unger, 2008; Ren, Ng, & Katzschner, 2011; Yang, Wang et al., 2020). The discrepancy between traditional urban landscape descriptions and urban climate classifications can be improved by studying LST heterogeneity based on LCZs (Kotharkar & Bagade, 2018; Lehnert, Geletič, Husák, & Vysoudil, 2014). However, due to the complexity of urban surfaces, the current researches on LCZ-LST are insufficient in depth and detail, and there are few achievements on the influence degree of factors on LST in each type of LCZ. Thus, to liminate uncertainty, this study uses building data in addition to remote sensing images for classifying natural and urban landscapes according to their surface attributes. Finally combined them together to explore the LST characteristics and influencing factors in different LCZ environments.

Urban development leads to local climate change (Yang, Luo et al., 2020). From a geographical perspective that emphasizes regional complexity, the aims of this study are: (1) Based on remote sensing and building data, identify and quantify the LST features of LCZ by GIS spatial analysis technology; (2) Construct parametric models and adopt statistical analysis method to explore the influencing factors of LST in each LCZ. The research outcomes can serve as a valuable reference for improving the urban thermal environment, construction of cool communities, and quality of human environments.

2. Data and methods

2.1. Overview of the study area

Shenyang, the capital city of Liaoning Province (Fig. 1), is an important central city in Northeast China, located between 122°25`–123°48`E and 41°12`–42°17`N. Its territory is dominated by plains, with a mountainous and hilly region in the southeast. Several rivers flow through the study area, and its climate is significantly affected by the monsoon, resulting in large temperature differences and distinct seasons. The annual average temperature is 6.2–9.7 ℃. The average temperature in summer reaches 29.0 ℃, while the average temperature in winter is -5.0 ℃. The urban area of Shenyang covers 3,495 km^2, and the primary urban districts include the Dadong, Huanggu, Hunnan, Shenhe, Heping, Shenbei, Tiexi, and Yuhong. Shenyang's economy has been developing rapidly in recent years, and its urbanization level is expected to reach 90 % by 2030. In this study, the characteristics and driving factors of thermal environment in Shenyang are analyzed to obtain reference for future urban planning.

2.2. Research data

The research data of the present study included Landsat8 OLI/TIRS, DEM, building, and meteorological data, as detailed in Table 1. Due to obvious seasonal changes in the study area and large temperature differences in a year, Landsat-8 images of different months over two years were obtained to attain a more reliable conclusion, and the periods with sunny weather and low cloud cover were selected. Remote sensing data were then processed in ENVI 5.3 for radiometric calibration and FLAASH atmospheric correction to eliminate the influence of atmosphere and light on ground object reflection. Meteorological data participated in the weather judgment and LST inversion of the day. In addition, based on Baidumap, building data were retrieved using Map vector downloader V3.0. After retrieval, the data were loaded into ArcGIS 10.2 to check. Almost no building blocks were lost, and the number of building floors was appended to the property table. The area and circumference at the bottom of the building contour were obtained using the computational geometry tool. In addition, DEM images were also as the supporting data for LCZ division.

2.3. Research methods

2.3.1. LST retrieval

The quality of remote sensing images will affect the accuracy of LST inversion. In the time period selected in our study, the precipitation was reduced and the weather was sunny, which usually makes the UHI effect more significant. The mono-window algorithm (Qin, Zhang, Karnieli, & Berliner, 2001) was then adopted to estimate the LST from Landsat8 TM10 band data (Hu, Qiao, & Wang, 2015) according to the following formulas:

$$T_s=(a(1\text{-}C\text{-}D)+(b(1\text{-}C\text{-}D)+C+D)\ T_{10}\text{-}DT_a)\ /(C\text{-}237.15) \tag{1}$$

$$C=\varepsilon\tau \tag{2}$$

$$D=(1\text{-}\tau)\ [1+(1\text{-}\varepsilon)\ \tau] \tag{3}$$

Here, T_s is the LST(K); T_{10} is the brightness temperature (K) on the sensor; T_a is the average temperature of the atmosphere (K); a and b are reference coefficients (when LST is in the range of 0–70 °C, a = −67.355351, b = 0.458606); ε is the land surface emissivity of T_{10}; τ is the atmospheric transmittance of T_{10}. Finally, the images were

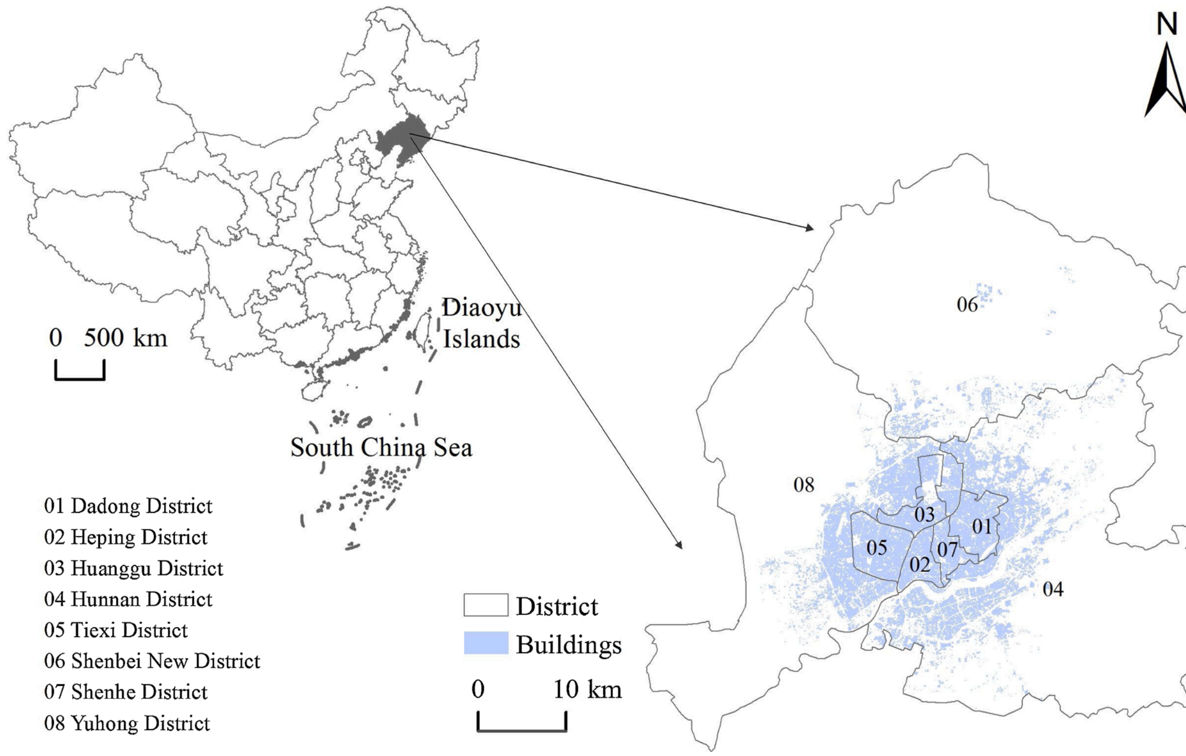

Fig. 1. The location of the study area.

Table 1
Data sources and descriptions.

Types	Description	Data sources	Sample
Remote Sensing data	Landsat8 OLI/TIRS (Date:2017-8-31,2017-12-21,2019-1-25,2019-9-22; Cloud cover: < 5%)	earthexplorer.usgs.gov	
	DEM (ASTGTM_N41E123, ASTGTM_N42E123)		
Building data	Building outline, contains height and floor	Baidumap	
Meteorological data	Meteorological site observation data (air temperature, air pressure, relative humidity)	rp5.ru	——

cropped according to the vector boundary of Shenyang.

2.3.2. LCZ division

The urban local climate system proposed by Stewart and Oke includes ten building types and seven land-cover types (Stewart & Oke, 2012). The built-up area of Shenyang covers an area of 560 km^2. Industrial areas are usually large low-rise buildings distributed outside the urban area, and the building structures of residential areas are mostly regular cubes. Our study is focused on community planning; therefore, we used the Create Fishnet tool in ArcGIS 10.2. Shenyang was divided into 60 m $\times$ 60 m grids for the research scale, and the buildings were mapped to the grid. Then, the grids were classified according to the number of building floors and density, and categorized as LCZ1–9. Factories were categorized as LCZ10 according to building function. Further, ENVI5.3 was used to construct a multi-source dataset based on the blue, green, red, and near-infrared bands of Landsat8, DEM, and the unsupervised classification results from the iterative self-organizing data analysis technique algorithm (ISODATA). The classification and regression tree (CART) algorithm was adopted to obtain the classification rules for LCZA-G. Due to large calculations, training samples were collected first. Then, parts of the typical areas were used as experimental areas to derive the decision tree, which was used to obtain the land-cover information of the entire study area. The detailed classifications are listed in Table 2.

2.3.3. Index calculation and correlation analysis

The influence of ventilation and heat dissipation on surface temperature is direct, and the different layouts of cities in horizontal and vertical directions lead to differences in surface temperature (Guo, Yang, Xiao et al., 2020). Based on previous studies, LST is usually higher in urban centers, and the relationship between resident buildings and LST is complicated (Morabito et al., 2016; Ren et al., 2016; Yang & Li, 2015). Vegetations and water are negatively correlated with LST (Deng et al., 2018, Chen & Zhang, 2017; Cici, 2020); However, the degree of correlation requires investigation under different LCZ circumstances. Moreover, the effects of urbanization on LST can be alleviated not only by balancing land use types, but also by optimizing urban form, which has a more significant effect (Yin, Yuan, Lu, Huang, & Liu, 2018). Thus, this study explores the relationship between LST and driving factors from two perspectives (i) the urban architectural layout (Wang, Cot, Adolphe, Geoffroy, & Sun, 2017) and (ii) remote sensing index (Xu, 2011). From these two perspectives, a total of nine influential indices were selected (Table3): the floor area ratio (FAR), plot ratio (PR), average building height (H), absolute rugosity (R), mean building volume (V_b), mean aspect ratio (λ_c), NDVI, BSI, and MNDWI.

The building form index was calculated based on a grid in ArcGIS 10.2, and the remote sensing index was calculated using the band math module in ENVI5.3. After excluding the extreme outliers, the correlation

Table 2
Local climate zone types (Stewart, Oke, & Krayenhoff, 2014).

Building LCZs		Nature LCZs	
	LCZ 1 Compact high-rise (more than 9 floors)	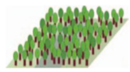	LCZ A Dense trees
	LCZ 2 Compact mid-rise(4–8 floors)	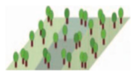	LCZ B Scattered trees
	LCZ 3 Compact low-rise(1–3 floors)	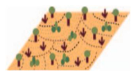	LCZ C Bush, scrub
	LCZ 4 Open high-rise (more than 9 floors)		LCZ D Low plants
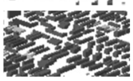	LCZ 5 Open mid-rise (4−8 floors)	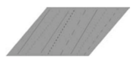	LCZ E Bare rock or paved
	LCZ 6 Open low-rise(1–3 floors)	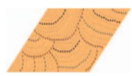	LCZ F Bare soil or sand
	LCZ 7 Sparse high-rise (more than 9 floors)		LCZ G Water
	LCZ 8 Sparse mid-rise (4−8 floors)		LCZ1–3: building density greater than 0.4 LCZ4–6: building density is between 0.2 and 0.4 LCZ7–9: building density less than 0.2
	LCZ 9 Sparse low-rise (1−3 floors)		
	LCZ10 Heavy industry		

analysis between LST and various indices was carried out in SPSS 24.0 software. The formula is as follows:

$$R = \frac{\sum(x-\overline{x})(y-\overline{y})}{\sqrt{\sum(x-\overline{x})^2}\sqrt{\sum(y-\overline{y})^2}} \tag{4}$$

In the formula, x and y are the observed values of the variables, while $\overline{x}$ and $\overline{y}$ are the mean values of the variables.

3. Results and analysis

3.1. Spatial distributions of LCZs and LSTs

Due to the significant spatiotemporal variation of LST, the four images are not displayed in a unified range classification (Fig. 2). Fig. 3 shows the proportion of land surface temperature in the study area. In the two summer images (Fig. 2(a), (d)), 82.79 % and 82.04 % of regional LST range between 21 °C and 30 °C, respectively. The city center shows a particularly high temperature. LST in the built-up area is mainly affected by the distribution of buildings, and the surface temperature in the southwest reaches 40 °C. The urban fringe areas outside the built-up areas are referred to as suburbs, where most of the LSTs are below 18 °C, and the low temperature areas are evident in the northwest and east. In contrast to summer, Shenyang winters are cold and dry, with scarce vegetation, and little difference in LST between urban and suburban areas. Most of the LSTs were approximately 0 °C (Fig. 2(b), (c)). In particular, some agricultural parks and resorts in the suburbs were relatively warm, with LSTs above 2 °C. In addition, an extremely low LST occurred in water bodies.

Fig. 4 and Tables 4 and 5 show that the eastern part of Shenyang City has lush vegetation, mostly natural forest land, and the main climatic zones are LCZA and LCZB. There are artificially rebuilt tourist development zones, forest parks, wetland parks, etc. LCZC was the main area in the north in summer, and the proportion of LCZF increased most in

Table 3
Calculation formula and significance of building form parameters and remote sensing index.

Types	formulas	Explanations
Urban morphology parameters	$FAR = \frac{\sum_i Ai}{S}$	Floor area ratio is defined as the ratio of footprint of the buildings to the overall site area.
	$PR = \frac{\sum_{ij}(Aij)}{S}$	Plot ratio is defined as the amount of construction permitted (in planning) on the land according to its size.
	$H = \frac{\sum_i (AiNi)\ \Delta H}{\sum_i Ai}$	This indicator is used for the description of the absolute rugosity of the terrain.
	$R = \frac{\sum_i (AiNi)\ \Delta H}{S}$	Absolute rugosity for a city is a parameter that describes the roughness of a surface to resist the free wind.
	$Vb = \frac{\sum_i Vbi}{N}$	This indicator can be used to describe the dispersion level of the buildings with different heights.
	$\lambda c = \frac{\sum_i Ei}{S}$	This indicator provides a connection between the building surface and the external environment.
Remote sensing indices	$NDVI = \frac{NIR - Red}{NIR + Red}$	An index related to vegetation cover that can reflect the growth status of vegetation.
	$MNDWI = \frac{Green - SWIR1}{Green + SWIR1}$	This is a modified normalized water index, which can solve the problem that cannot distinguish between building and water information.
	$BSI = \frac{(SWIR1 + Red) - (NIR + Blue)}{(SWIR1 + Red) + (NIR + Blue)}$	The high reflectivity of bare soil in the mid–infrared band was used to extract bare soil information.

Note: Ai is the floor area of the first floor of the i-th building; Ni is the number of floors; Aij is the area of the j-th floor of the i-th building; △H is the average height, which is usually 3 m; S is the total land area, i.e., the unit grid area; Vbi is the volume of the i-th building; N is the total number of buildings; Ei is the enclosure area of the i-th building, including all exterior walls and roof surfaces.

the winter. Large industrial buildings are distributed outside the city center, and LCZ10 proportion in 2019 is 0.81 % lower than that in 2017. As the old areas with early development, Heping, Shenhe, and Huanggu District city facilities are complete and almost filled with buildings. In 2017, LCZs of residential areas accounted for LCZ9 > LCZ6 > LCZ5 > LCZ8 > LCZ3 > LCZ2 > LCZ7 > LCZ4 > LCZ1. In 2019, LCZs occupied LCZ 9 > LCZ 5 > LCZ3 > LCZ6 > LCZ8 > LCZ7 > LCZ2 > LCZ4 > LCZ1. Middle and low-rise buildings accounted for the majority, with high-rise buildings LCZ1, LCZ4, and LCZ7 increasing by 1.22 %, 1.80 %, and 1.39 %, respectively, from 2017 to 2019.

3.2. Differences in LSTs based on LCZs

To explore the conditions of LCZs reflected in the urban thermal environment, the typical characteristics of LSTs exhibited in each LCZ were analyzed in this study. The results show that the LSTs of different LCZs are significantly different (Fig. 5). In the building type LCZ, emissions from industrial plant operations resulted in a consistently high LST in LCZ10. For residential areas, buildings are distributed in different densities in the horizontal direction and in different heights in the vertical direction, as well as different ventilation and heat dissipation

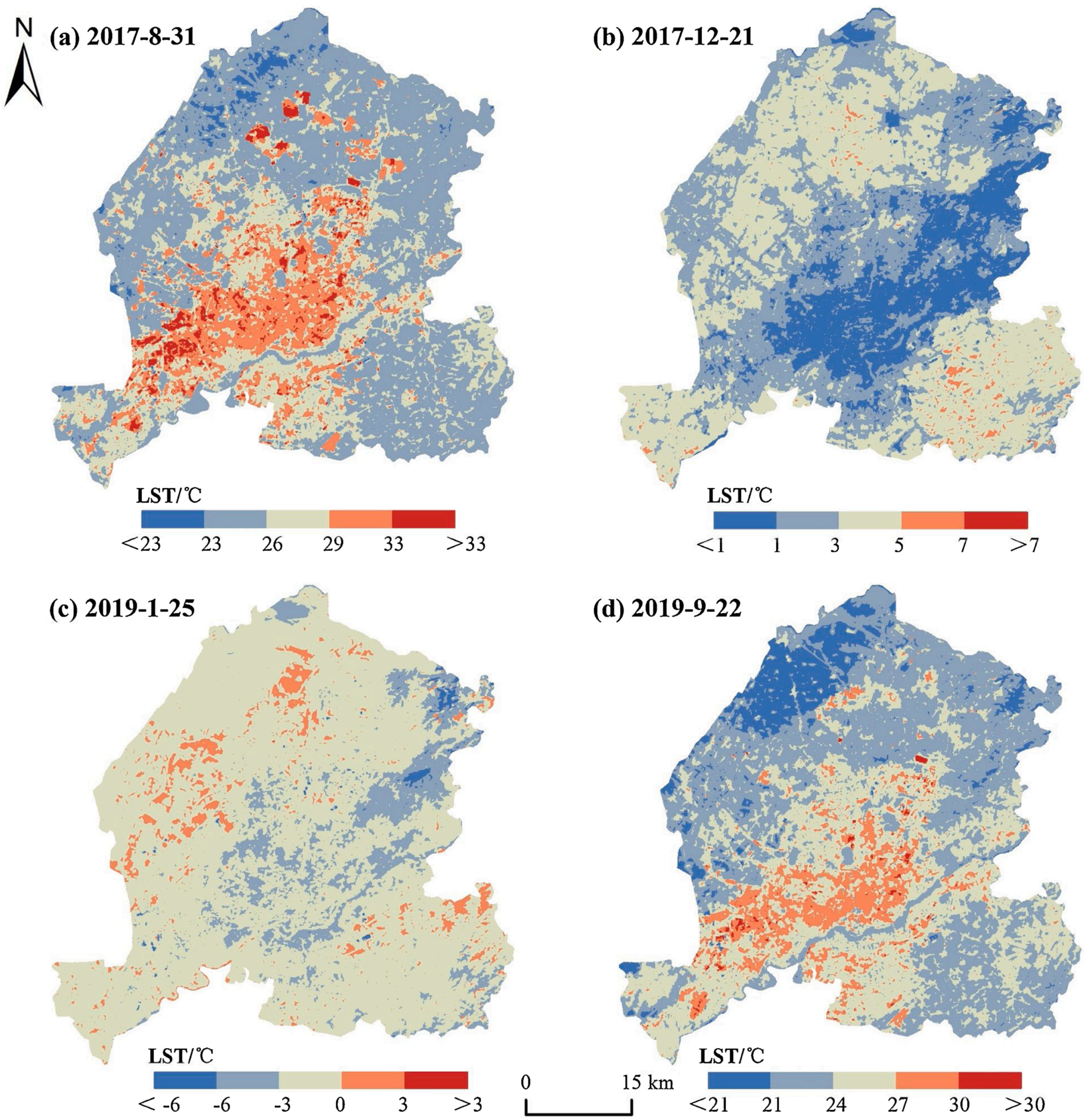

Fig. 2. Spatial distribution of land surface temperature in Shenyang.

spaces. As a result, LST is affected, which is more obvious in summer. The highest average LST occurred in LCZ2 in summer, 33.26 °C in 2017 and 28.19 °C in 2019. LCZ3 and LCZ5 were second only to LCZ2. The average LST in 2017 was 33.09 °C and 31.92 °C, respectively, and in 2019 was 27.04 °C and 26.53 °C, respectively. The LST of LCZ1, LCZ4, and LCZ7 in building LCZs is relatively low. The natural LCZ has a significant influence on LST in winter. The average LST in 2017 was LCZF > LCZB > LCZC > LCZD > LCZA > LCZE > LCZG, and the average LST in 2019 was LCZF > LCZC > LCZB > LCZE > LCZD > LCZG > LCZA. Therefore, exposed soil and hardened pavement are more likely to increase LST, whereas high-density vegetation and water are more likely to decrease LST.

3.3. Analysis of LST impact factors

The four groups of data were summarized into data sets and outliers were removed for statistical analysis to obtain the average value of indicators in each LCZ (Table 6). Using the combined information from the datasets and the box-plots (Fig. 5), it can be inferred that the LST is higher overall for the intensive building area where the average FAR exceeds 0.59. When the FAR is roughly the same, the LST in the middle-level building with a height of approximately 20 m was the highest. LCZ7 has a significant cooling, but its average H was the highest. Table 7 lists the correlation coefficients between LSTs and the impact factors in each LCZ. The degree of correlation differs in different LCZs, indicating that varying LCZ types have different degrees of impact on the LSTs. The buildings are an important driving factor for increased LST. The urban center of Shenyang has tall and dense buildings, a relatively low level of scattering, and rough and complex surfaces. As the coverage increases in the horizontal direction, the single or combined structure of buildings becomes more complicated, and the airflow rate decreases, which is not conducive to heat diffusion. The LST was always positively correlated with the FAR, with the lowest correlation coefficient of 0.271 in LCZ8, and the highest correlation coefficient of 0.682 in LCZ2. As the building height increases, airflow is obstructed in the vertical direction, which likely increases the LST. Notably, the LST of low-rise buildings,

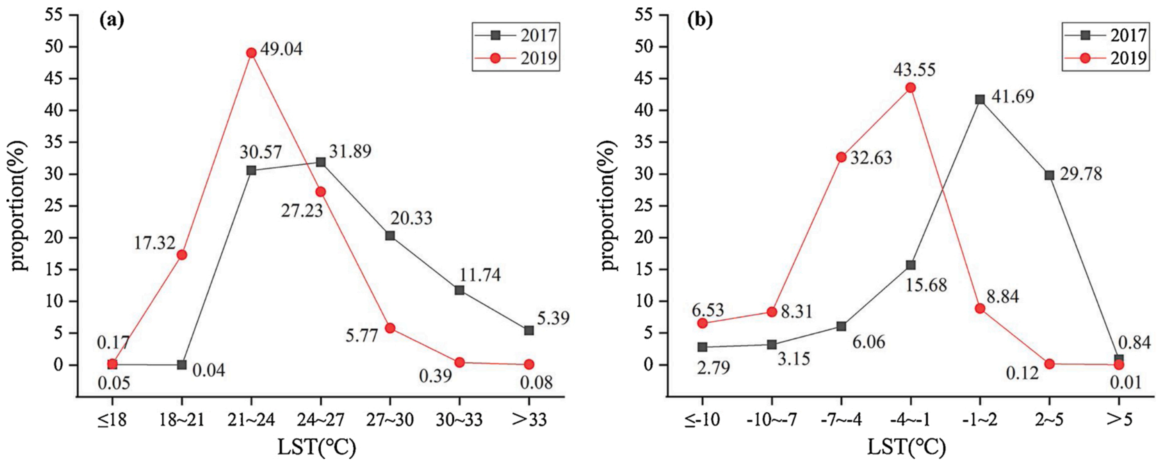

Fig. 3. LST numerical statistics in summer (a) and winter (b).

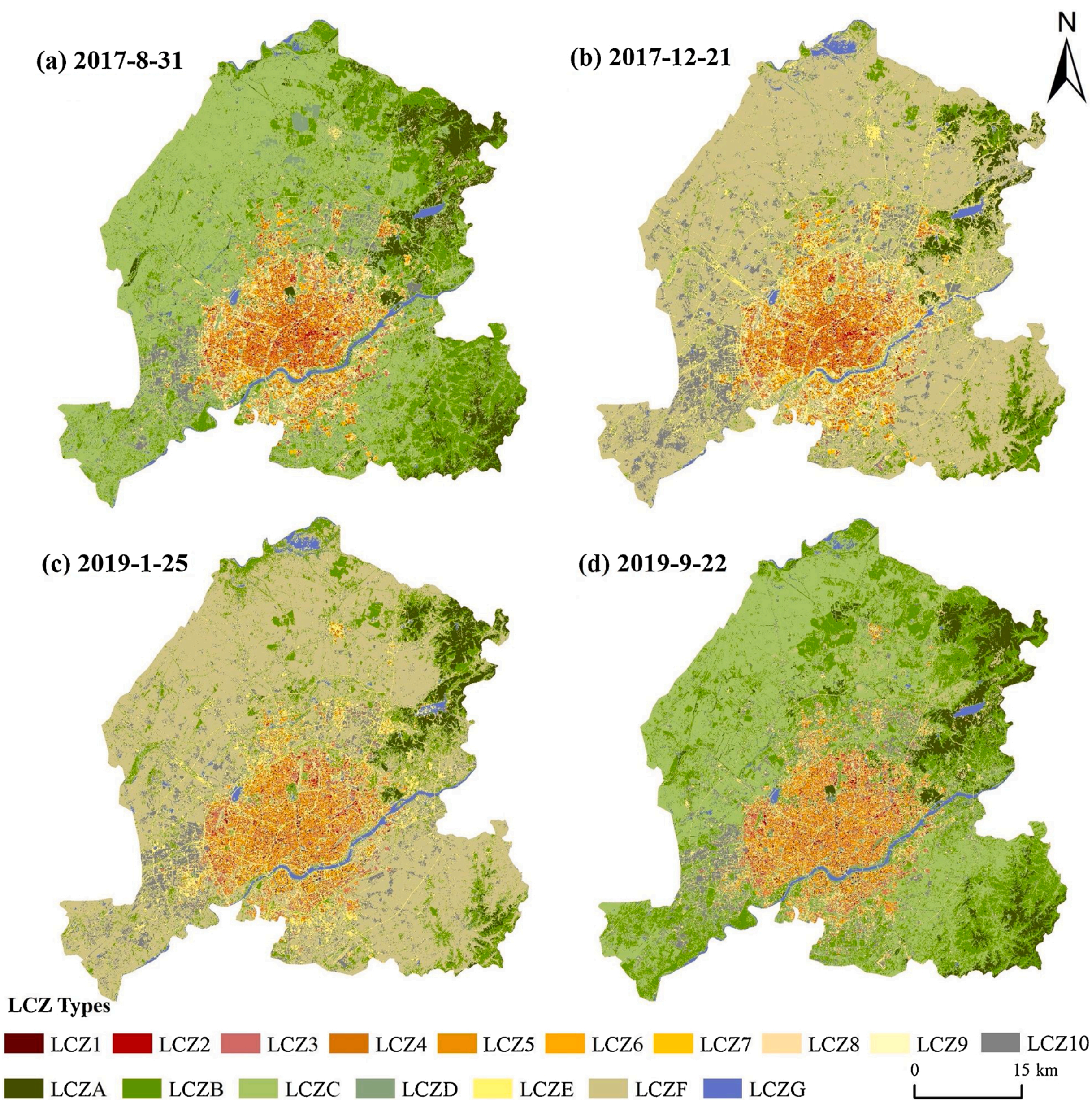

Fig. 4. Classification map of local climate zones in Shenyang.

Table 4
Percentage of built LCZs.

	LCZ1	LCZ2	LCZ3	LCZ4	LCZ5	LCZ6	LCZ7	LCZ8	LCZ9	LCZ10
2017	0.98%	5.36 %	10.28 %	3.53 %	17.51 %	21.53 %	4.68 %	10.81 %	23.89 %	1.45 %
2019	2.20%	3.58 %	16.41 %	5.33 %	17.06 %	15.67 %	6.07 %	12.33 %	20.71 %	0.64 %

Table 5
Percentage of nature LCZs.

	LCZA	LCZB	LCZC	LCZD	LCZE	LCZF	LCZG
2017-8-31	9.20%	25.31 %	22.51 %	26.01 %	14.01 %	1.58 %	1.38 %
2017-12-21	1.54%	18.00 %	31.40 %	4.29 %	21.95 %	20.19 %	2.62 %
2019-1-25	1.47%	16.11 %	28.51 %	4.64 %	24.53 %	21.23 %	3.49 %
2019-9-22	7.38%	29.36 %	32.29 %	10.10 %	13.28 %	5.79 %	1.81 %

including LCZ3, LCZ6, and LCZ9, was positively correlated with H, whereas the LST of high-rise and middle-level buildings was negatively correlated with H; LCZ3 exhibits the highest degree of positive correlation at 0.421, whereas LCZ7 exhibits the highest degree of negative correlation at -0.706. The heat inside the city tends to be blocked by dense mid- and high-rise buildings; however, when the building density reaches a certain level within a reasonable range, the buildings block a portion of the solar radiation. As a result, compared with dense low-rise buildings, sparse high-rise buildings have a lower LST.

For the normalized remote sensing indices, LST had the strongest correlation with NDVI (-0.890) in LCZF, the strongest correlation with MNDWI (-0.737) in LCZA, and a relatively strong correlation with BSI (0.803) in LCZD. These results show that bare soil in vegetation coverage areas can increase the LST, whereas vegetation and water sources in bare soil areas can significantly reduce the LST.

4. Discussion

Due to the complexity of cities, the regional thermal environment cannot be studied using the traditional UHI definition based on the temperature difference between urban and rural areas (Oke, 1973). This

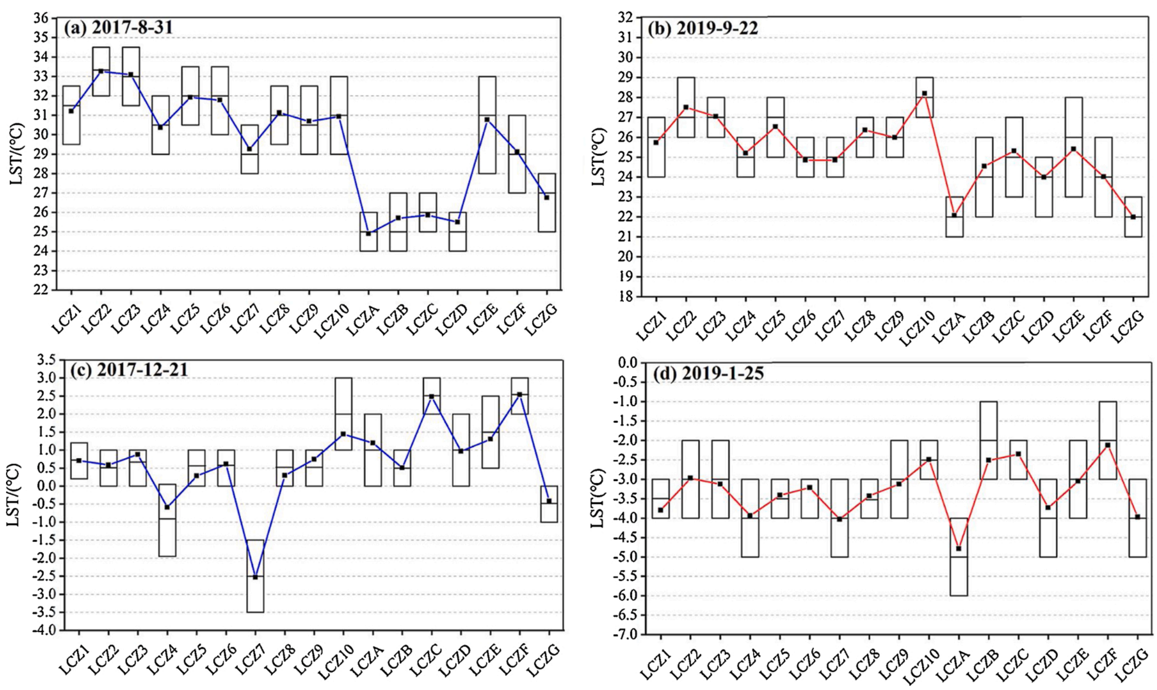

Fig. 5. Box-plots with LSTs in LCZs in 2017 (a,c) and 2019 (b,d): The line within the box indicates the median; The rectangular indicates the average; The bottom of the box is the first quartile and the top is the third quartile.

Table 6
Mean values of indicators for each LCZ.

	FAR	H(m)	PR	$V_b(km^2)$	λ_c	R		NDVI	MNDWI	BSI
LCZ1	0.61	49.80	9.72	4.70	5.07	29.17	LCZA	0.42	0.19	−0.14
LCZ2	0.59	20.85	2.59	2.82	1.83	9.88	LCZB	0.28	0.16	−0.17
LCZ3	0.60	7.67	2.49	1.12	1.81	7.38	LCZC	0.26	−0.11	−0.28
LCZ4	0.29	45.63	4.29	2.59	2.84	12.87	LCZD	0.29	−0.09	−0.13
LCZ5	0.27	21.61	1.90	1.93	1.52	5.69	LCZE	0.08	−0.03	0.21
LCZ6	0.23	8.76	1.05	0.41	1.02	3.15	LCZF	0.14	−0.13	0.86
LCZ7	0.10	53.87	1.74	1.25	1.66	5.23	LCZG	0.06	0.31	−0.09
LCZ8	0.11	19.39	0.73	0.43	0.78	3.19	——			
LCZ9	0.09	7.52	0.25	0.14	0.34	0.75				
LCZ10	0.26	4.25	0.43	0.30	0.47	1.29				

Table 7
Correlation coefficient between LST and impact factors.

	FAR	H	PR	V_b	λ_c	R		NDVI	MNDWI	BSI
LCZ1	0.570	−0.612	0.488	−0.372	−0.546	−0.483	LCZA	−0.493	−0.737	0.768
LCZ2	0.682	−0.454	0.402	0.873	−0.655	−0.445	LCZB	−0.703	−0.592	0.670
LCZ3	0.583	0.421	0.455	0.205	0.504	0.347	LCZC	−0.777	−0.661	0.512
LCZ4	0.560	−0.429	0.051	−0.446	−0.213	−0.429	LCZD	−0.800	−0.273	0.803
LCZ5	0.678	−0.392	0.167	−0.453	−0.193	−0.565	LCZE	−0.499	−0.452	0.535
LCZ6	0.330	0.209	0.124	0.163	0.359	0.176	LCZF	−0.890	−0.262	0.759
LCZ7	0.441	−0.706	0.271	−0.642	−0.164	−0.630	LCZG	−0.529	−0.355	0.413
LCZ8	0.271	−0.676	0.435	−0.576	−0.329	−0.598	—			
LCZ9	0.459	0.137	0.370	0.095	0.591	0.271				
LCZ10	0.422	−0.164	0.403	0.426	0.459	0.431				

problem, however, can be optimized using the local climate system (Zhao, 2018). Building structure parameters and normalized remote sensing indices can effectively reflect the characteristics of urban internal structures (Bernard et al., 2018a, 2018b; Hu & Brunsell, 2013). By assessing the correlations of building structure and land cover with LST at the LCZ scale, the impact factors for the urban climate can be identified. The results of this study can serve as a reference for regional building layout planning. In contrast, vegetation can help cool urban centers (Turner-Skoff & Cavender, 2019). While humans are pursuing concentrated development, vegetation density in cities has decreased (Brown et al., 2018; Qiao, Tian, & Xiao, 2013). Therefore, to achieve sustainable development of cities, attention should be paid to the environmental and social benefits of trees as well as their importance for cooling the environment.

4.1. LCZ temperature differences

LCZ is becoming a common objective classification system for the urban climate in urban thermal environment research (Abdi, Hami, & Zarehaghi, 2020; Bechtel et al., 2019; Yang, Sun, Ge, & Li, 2017). In terms of research on temperature differences, the results indicate that the LST changes significantly with building-type LCZs. Among the natural-type LCZs, bare land has the highest LST, whereas water bodies and forests exhibit a certain cooling effect (Mu, Liu, Zhang, Han, & Yang, 2019). Under ideal weather conditions, vegetation coverage areas and sparse low-rise building areas can have a temperature difference of 1.5 °C. The average LST of building-type LCZs is 4 °C higher than that of natural-type LCZs (Alexander & Mills, 2014). Fig. 6 shows the mean LST difference between a pair of LCZs in summer 2017 (vertical axis minus horizontal axis); the darkest cells represent the temperature difference areas between building-type LCZs and natural-type LCZs (upper right and lower left). Under the same conditions, climate zone types with temperature differences above 5 °C are concentrated between LCZ1-6 and LCZA-D. In the area of building-type LCZs (upper left), LCZ2 and LCZ3 are a darker red, and in the area of natural-type LCZs (lower right), LCZE and LCZF are a darker green.

4.2. Urban thermal environment optimization scheme

A comparison of the relationships between building height/spacing and LST indicates that the local thermal environment was predominantly determined by the building density, and the building height/

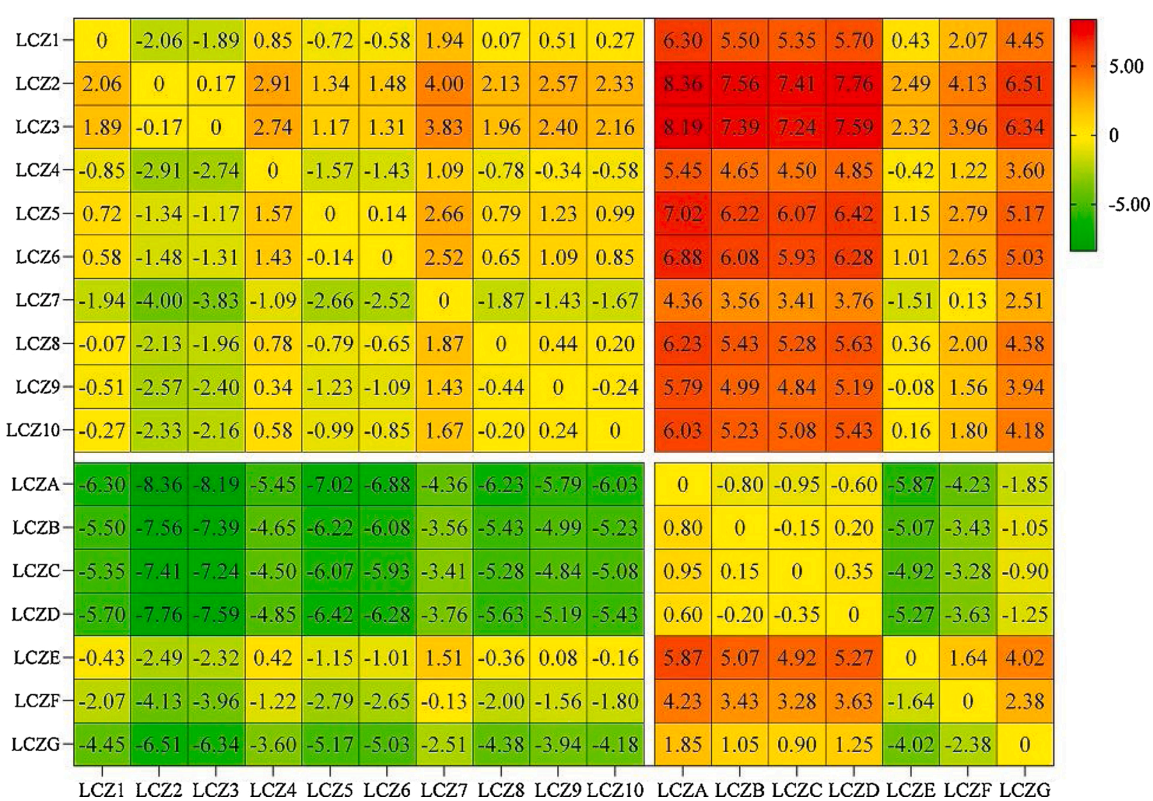

Fig. 6. The mean LST differences (°C) between a pair of LCZs in the summer of 2017.

width ratio was inversely proportional to LST (Chen, Lin, & Lin, 2017; Deng & Wong, 2020). The results of this research show that correlations between the building height/width ratio and LST vary in different climate zones. The mean aspect ratio was inversely proportional to LST in most cases, whereas it was proportional to LST in LCZ3, LCZ6, and LCZ9. Furthermore, as the LST may be affected by many factors, weak correlations were observed between different indices. The global autocorrelation Moran's I value of LST was above 0.7, and its spatial distribution had a strong correlation with the spatial variables (e.g., land use) but a weak correlation with the building structure (Guo, Yang, Xiao et al., 2020); In this study, a 60 m × 60 m grid was used to divide the LCZs, and the building structure indices were calculated based on the grid, which improved the research accuracy. In the actual planning of building layout, the land area occupied by buildings should be fully considered, and an appropriate scale should be employed for reasonable design (Liu, Fang, Xu, Zhang, & Luan, 2017). The correlation coefficients between LST and building structure indices were generally above 0.5 in each climatic zone. Moreover, FAR and H had the most evident changes in correlation with LST. If the area is small, buildings may be dense. Therefore, the urban environment should be built by increasing the number of floors (higher than four floors) and establishing green belts. Moreover, cool communities should be constructed at a distance from industrial intensive areas and make full use of the distribution of vegetation and water to form a harmonious and comfortable living environment (Xue et al., 2019).

4.3. Limitations

The LCZ division based on land-cover types employed in this study may have certain errors due to technical limitations and cannot accurately match the actual situation. Furthermore, cities comprehensively influence LST. Building form, land-cover factors, differences in building materials, population, social economy, and other aspects of cities with different structures and scales will all contribute to varying thermal environments; thus, the grid scale selection will also affect the correlation degree. Therefore, subsequent studies can compare the relationship between LST and driving factors at different grid scales to draw broader conclusions.

5. Conclusions

Compared with global warming, changes in LST more directly affect human residential comfort levels. In this study, Landsat8 remote sensing images and Shenyang building data were used to analyze the spatial distribution characteristics of LST and its impact factors based on the LCZ system. The conclusions are as follows.

(1) The spatial distribution of LCZs is consistent with that of LSTs. The LSTs of buildings and bare-land areas are higher than those of areas covered by vegetation and water bodies.
(2) The LST ranged from 24.90 °C (LCZA) to 33.26 °C (LCZ2) in the summer of 2017 and from 2.53 °C (LCZ7) to 2.89 °C (LCZ3) in winter; the LST ranged from 22.00 °C (LCZ2) to 28.19 °C (LCZE) in summer 2019, and from -4.79 °C (LCZ10) to -2.12 °C (LCZ3) in winter.
(3) Different climate zones have different impacts on the LST. The distribution of buildings in the three-dimensional urban space is an important driving factor for increasing LST. The LST is always positively correlated with the FAR, with the lowest correlation coefficient of 0.271 in LCZ8, and the highest correlation coefficient of 0.682 in LCZ2. The LST exhibits negative correlation with H in high-rise and middle-level buildings, and a positive correlation in LCZ3, LCZ6, and LCZ9. The highest degree of positive correlation of 0.421 is in LCZ3, whereas the highest degree of negative correlation of -0.706 is in LCZ7. Water bodies and vegetation in the city have a certain cooling effect on the surrounding environment, whereas bare land and paved roads cause the LST to rise. Therefore, during urban construction, building height can be appropriately increased while reducing the building density, vegetation and water body distributions should be arranged rationally to build cool areas, and measures should be taken to suit local conditions, thereby ensuring the coordinated development of regional climate and social economy.

Declaration of Competing Interest

The authors report no declarations of interest.

Acknowledgements

This research study was supported by the National Natural Science Foundation of China (grant no. 41771178, 41630749, 41471140), Liaoning Province Innovative Talents Support Program (grant no. LR2017017), and the Liaoning Province Outstanding Youth Program (grant no. LJQ2015058). The authors would like to acknowledge all experts' contributions in the building of the model and the formulation of the strategies in this study.

References

Abdi, B., Hami, A., & Zarehaghi, D. (2020). Impact of small-scale tree planting patterns on outdoor cooling and thermal comfort. *Sustainable Cities and Society, 56*, Article 102085.
Alexander, P., & Mills, G. (2014). Local climate classification and Dublin's urban heat island. *Atmosphere, 5*, 755–774.
Amiri, R., Weng, Q., Alimohammadi, A., & Alavipanah, S. K. (2009). Spatial–temporal dynamics of land surface temperature in relation to fractional vegetation cover and land use/cover in the Tabriz urban area, Iran. *Remote Sensing of Environment, 113*, 2606–2617.
Bartesaghi Koc, C., Osmond, P., Peters, A., & Irger, M. (2018). Understanding land surface temperature differences of local climate zones based on airborne remote sensing data. *IEEE Journal of Selected Topics in Applied Earth Observations and Remote Sensing, 11*, 2724–2730.
Bechtel, B., Alexander, P., Böhner, J., Ching, J., Conrad, O., Feddema, J., et al. (2015). Mapping local climate zones for a worldwide database of the form and function of cities. *ISPRS International Journal of Geo-Information, 4*, 199–219.
Bechtel, B., Demuzere, M., Mills, G., Zhan, W., Sismanidis, P., Small, C., et al. (2019). SUHI analysis using local climate zones—A comparison of 50 cities. *Urban Climate, 28*, Article 100451.
Bernard, J., Bocher, E., Petit, G., & Palominos, S. (2018a). Sky view factor calculation in urban context: Computational performance and accuracy analysis of two open and free GIS tools. *Climate, 6*, 60.
Bernard, J., Bocher, E., Petit, G., & Palominos, S. (2018b). Sky view factor calculation in urban context: Computational performance and accuracy analysis of two open and free GIS tools. *Climate*, 6.
Brown, H., Proust, K., Newell, B., Spickett, J., Capon, T., & Bartholomew, L. (2018). Cool communities-urban density, trees, and health. *International Journal of Environmental Research and Public Health, 15*, 1547.
Budhiraja, B., Gawuc, L., & Agrawal, G. (2019). Seasonality of surface urban heat island in Delhi City region measured by local climate zones and conventional indicators. *IEEE Journal of Selected Topics in Applied Earth Observations and Remote Sensing, 12*, 5223–5232.
Chen, Y. C., Lin, T. P., & Lin, C. T. (2017). A simple approach for the development of urban climatic maps based on the urban characteristics in Tainan. *International Journal of Biometeorology, 61*, 1029–1041.
Chen, Z., Yu, B., Zhou, Y., Liu, H., Yang, C., Shi, K., et al. (2019). Mapping global urban areas from 2000 to 2012 using time-series nighttime light data and MODIS products. *IEEE Journal of Selected Topics in Applied Earth Observations and Remote Sensing, 12*, 1143–1153.
Chen, X., & Zhang, Y. (2017). Impacts of urban surface characteristics on spatiotemporal pattern of land surface temperature in Kunming of China. *Sustainable Cities and Society, 32*, 87–99.
Cici, A. (2020). Normalised difference spectral indices and urban land cover as indicators of land surface temperature (LST). *International Journal of Applied Earth Observations and Geoinformation*, 86.
Deng, J. Y., & Wong, N. H. (2020). Impact of urban canyon geometries on outdoor thermal comfort in central business districts. *Sustainable Cities and Society, 53*, Article 101966.
Deng, Y., Wang, S., Bai, X., Tian, Y., Wu, L., Xiao, J., et al. (2018). Relationship among land surface temperature and LUCC, NDVI in typical karst area. *Scientific Reports*, 8.
Emmanuel, R., & Krüger, E. (2012). Urban heat island and its impact on climate change resilience in a shrinking city: The case of Glasgow, UK. *Building and Environment, 53*, 137–149.

Estoque, R. C., Murayama, Y., & Myint, S. W. (2017). Effects of landscape composition and pattern on land surface temperature: An urban heat island study in the megacities of Southeast Asia. *The Science of the Total Environment, 577*, 349–359.
Gál, T., Lindberg, F., & Unger, J. (2008). Computing continuous sky view factors using 3D urban raster and vector databases: Comparison and application to urban climate. *Theoretical and Applied Climatology, 95*, 111–123.
Gilbert, H., Mandel, B. H., & Levinson, R. (2016). Keeping California cool: Recent cool community developments. *Energy and Buildings, 114*, 20–26.
Gulbe, L., Caune, V., & Korats, G. (2017). Urban area thermal monitoring: Liepaja case study using satellite and aerial thermal data. *International Journal of Applied Earth Observation and Geoinformation, 63*, 45–54.
Guo, A., Yang, J., Sun, W., Xiao, X., Xia, J., Jin, C., et al. (2020). Impact of urban morphology and landscape characteristics on spatiotemporal heterogeneity of land surface temperature. *Sustainable Cities and Society, 63*, Article 102443.
Guo, A., Yang, J., Xiao, X., Xia, J., Jin, C., & Li, X. (2020). Influences of urban spatial form on urban heat island effects at the community level in China. *Sustainable Cities and Society, 53*, 1–12.
He, B. J. (2018). Potentials of meteorological characteristics and synoptic conditions to mitigate urban heat island effect. *Urban Climate, 24*, 26–33.
He, B. J., Ding, L., & Prasad, D. (2019). Enhancing urban ventilation performance through the development of precinct ventilation zones: A case study based on the Greater Sydney, Australia. *Sustainable Cities and Society, 47*, Article 101472.
He, B. J., Wang, J., Liu, H., & Ulpiani, G. (2021). Localized synergies between heat waves and urban heat islands: Implications on human thermal comfort and urban heat management. *Environmental Research, 193*, 110584.
Hu, L., & Brunsell, N. A. (2013). The impact of temporal aggregation of land surface temperature data for surface urban heat island (SUHI) monitoring. *Remote Sensing of Environment, 134*, 162–174.
Hu, D., Qiao, K., & Wang, X. (2015). Land surface temperature retrieval from Landsat 8 thermal infrared data using mono-window algorithm. *Journal of Remote Sensing, 19*, 964–976.
Hu, J., Yang, Y., Pan, X., Zhu, Q., Zhan, W., Wang, Y., et al. (2019). Analysis of the spatial and temporal variations of land surface temperature based on local climate zones: A case study in Nanjing, China. *IEEE Journal of Selected Topics in Applied Earth Observations and Remote Sensing, 12*, 4213–4223.
Kong, L., Lau, K. K.-L., Yuan, C., Chen, Y., Xu, Y., Ren, C., et al. (2017). Regulation of outdoor thermal comfort by trees in Hong Kong. *Sustainable Cities and Society, 31*, 12–25.
Kotharkar, R., & Bagade, A. (2018). Evaluating urban heat island in the critical local climate zones of an Indian city. *Landscape and Urban Planning, 169*, 92–104.
Krayenhoff, E., & Voogt, J. (2016). Daytime thermal anisotropy of urban neighbourhoods: Morphological causation. *Remote Sensing, 8*, 108.
Lehnert, M., Geletič, J., Husák, J., & Vysoudil, M. (2014). Urban field classification by "local climate zones" in a medium-sized Central European city: The case of Olomouc (Czech Republic). *Theoretical and Applied Climatology, 122*, 531–541.
Li, F., Yan, Q., Bian, Z., Liu, B., & Wu, Z. (2020). A POI and LST adjusted NTL urban index for urban built-up area extraction. *Sensors (Basel), 20*, 2918.
Liu, Y., Fang, X., Xu, Y., Zhang, S., & Luan, Q. (2017). Assessment of surface urban heat island across China's three main urban agglomerations. *Theoretical and Applied Climatology, 133*, 473–488.
Ma, T., Zhou, Y., Zhou, C., Haynie, S., Pei, T., & Xu, T. (2015). Night-time light derived estimation of spatio-temporal characteristics of urbanization dynamics using DMSP/OLS satellite data. *Remote Sensing of Environment, 158*, 453–464.
Morabito, M., Crisci, A., Messeri, A., Orlandini, S., Raschi, A., Maracchi, G., et al. (2016). The impact of built-up surfaces on land surface temperatures in Italian urban areas. *The Science of the Total Environment, 551-552*, 317–326.
Mu, K., Liu, Y., Zhang, M., Han, B., & Yang, L. (2019). Investigations of surface urban heat island effect based on local climate zone method: A case of Xi'an. *E3S Web of Conferences, 136*, 05011.
Ochola, E. M., Fakharizadehshirazi, E., Adimo, A. O., Mukundi, J. B., Wesonga, J. M., & Sodoudi, S. (2020). Inter-local climate zone differentiation of land surface temperatures for management of urban heat in Nairobi City, Kenya. *Urban Climate, 31*, Article 100540.
Oke, T. R. (1973). City size and the urban heat island. *Atmospheric Environment, 7*, 769–779.
Panagopoulos, T., Gonzalez Duque, J. A., & Bostenaru Dan, M. (2016). Urban planning with respect to environmental quality and human well-being. *Environmental Pollution, 208*, 137–144.
Portela, C. I., Massi, K. G., Rodrigues, T., & Alcântara, E. (2020). Impact of urban and industrial features on land surface temperature: Evidences from satellite thermal indices. *Sustainable Cities and Society, 56*, Article 102100.
Qiao, Z., Huang, N., Xu, X., Sun, Z., Wu, C., & Yang, J. (2019). Spatio-temporal pattern and evolution of the urban thermal landscape in metropolitan Beijing between 2003 and 2017. *Acta Geographica Sinica, 74*, 475–489.
Qiao, Z., Tian, G., & Xiao, L. (2013). Diurnal and seasonal impacts of urbanization on the urban thermal environment: A case study of Beijing using MODIS data. *ISPRS Journal of Photogrammetry and Remote Sensing, 85*, 93–101.
Qin, Z., Zhang, M., Karnieli, A., & Berliner, P. (2001). Mono-window algorithm for retrieving land surface temperature from Landsat TM6 data. *Acta Geographica Sinica, 68*, 456–466.
Ren, C., Ng, E. Y.-y., & Katzschner, L. (2011). Urban climatic map studies: A review. *International Journal of Climatology, 31*, 2213–2233.
Ren, Y., Deng, L. Y., Zuo, S. D., Song, X. D., Liao, Y. L., Xu, C. D., et al. (2016). Quantifying the influences of various ecological factors on land surface temperature of urban forests. *Environmental Pollution*, 1–11.
Shi, Y., Lau, K. K. L., Ren, C., & Ng, E. (2018). Evaluating the local climate zone classification in high-density heterogeneous urban environment using mobile measurement. *Urban Climate, 25*, 167–186.
Song, J., Du, S., Feng, X., & Guo, L. (2014). The relationships between landscape compositions and land surface temperature: Quantifying their resolution sensitivity with spatial regression models. *Landscape and Urban Planning, 123*, 145–157.
Stewart, I. D., & Oke, T. R. (2012). Local climate zones for urban temperature studies. *Bulletin of the American Meteorological Society, 93*, 1879–1900.
Stewart, I. D., Oke, T. R., & Krayenhoff, E. S. (2014). Evaluation of the' local climate zone' scheme using temperature observations and model simulations. *International Journal of Climatology, 34*, 1062–1080.
Thomas, G., Sherin, A. P., Ansar, S., & Zachariah, E. J. (2014). Analysis of urban heat island in Kochi, India, using a modified local climate zone classification. *Procedia Environmental Sciences, 21*, 3–13.
Turner-Skoff, J. B., & Cavender, N. (2019). The benefits of trees for livable and sustainable communities. *Plants, People, Planet, 1*, 323–335.
Tv, R., Aithal, B. H., & Sanna, D. D. (2012). Insights to urban dynamics through landscape spatial pattern analysis. *International Journal of Applied Earth Observation and Geoinformation, 18*, 329–343.
Unger, J., Lelovics, E., & Gál, T. (2014). Local climate zone mapping using GIS methods in Szeged. *Hungarian Geographical Bulletin, 63*, 29–41.
Wang, J., & Ouyang, W. (2017). Attenuating the surface urban heat island within the local thermal zones through land surface modification. *Journal of Environmental Management, 187*, 239–252.
Wang, B., Cot, L. D., Adolphe, L., Geoffroy, S., & Sun, S. (2017). Cross indicator analysis between wind energy potential and urban morphology. *Renewable Energy, 113*, 989–1006.
Xie, P., Yang, J., Wang, H., Liu, Y., & Liu, Y. (2020). A new method of simulating urban ventilation corridors using circuit theory. *Sustainable Cities and Society, 59*, Article 102162.
Xu, H. (2011). Analysis on urban heat island effect based on the dynamics of urban surface biophysical descriptors. *Acta Ecologica Sinica, 31*, 3890–3901.
Xue, Z., Hou, G., Zhang, Z., Lyu, X., Jiang, M., Zou, Y., et al. (2019). Quantifying the cooling-effects of urban and peri-urban wetlands using remote sensing data: Case study of cities of Northeast China. *Landscape and Urban Planning, 182*, 92–100.
Yang, X., & Li, Y. (2015). The impact of building density and building height heterogeneity on average urban albedo and street surface temperature. *Building and Environment, 90*, 146–156.
Yang, J., Jin, S., Xiao, X., Jin, C., Xia, J., Li, X., et al. (2019). Local climate zone ventilation and urban land surface temperatures: Towards a performance-based and wind-sensitive planning proposal in megacities. *Sustainable Cities and Society, 47*, Article 101487.
Yang, J., Luo, X., Jin, C., Xiao, X., & Xia, J. (2020). Spatiotemporal patterns of vegetation phenology along the urban–rural gradient in Coastal Dalian, China. *Urban Forestry & Urban Greening, 54*, Article 126784.
Yang, X., Ruby Leung, L., Zhao, N., Zhao, C., Qian, Y., Hu, K., et al. (2017). Contribution of urbanization to the increase of extreme heat events in an urban agglomeration in east China. *Geophysical Research Letters, 44*, 6940–6950.
Yang, J., Sun, J., Ge, Q., & Li, X. (2017). Assessing the impacts of urbanization-associated green space on urban land surface temperature: A case study of Dalian, China. *Urban Forestry & Urban Greening, 22*, 1–10.
Yang, J., Wang, Y., Xiao, X., Jin, C., Xia, J., & Li, X. (2019). Spatial differentiation of urban wind and thermal environment in different grid sizes. *Urban Climate, 28*, Article 100458.
Yang, J., Wang, Y., Xiu, C., Xiao, X., Xia, J., & Jin, C. (2020). Optimizing local climate zones to mitigate urban heat island effect in human settlements. *Journal of Cleaner Production, 275*, Article 123767.
Yang, B., Yang, X., Leung, L. R., Zhong, S., Qian, Y., Zhao, C., et al. (2019). Modeling the impacts of urbanization on summer thermal comfort: The role of urban land use and anthropogenic heat. *Journal of Geophysical Research: Atmospheres, 124*. https://doi.org/10.1029/2018JD029829
Yang, J., Zhan, Y., Xiao, X., Xia, J. C., Sun, W., & Li, X. (2020). Investigating the diversity of land surface temperature characteristics in different scale cities based on local climate zones. *Urban Climate, 34*, Article 100700.
Yin, C., Yuan, M., Lu, Y., Huang, Y., & Liu, Y. (2018). Effects of urban form on the urban heat island effect based on spatial regression model. *The Science of the Total Environment, 634*, 696–704.
You, H., Yang, J., Xue, B., Xiao, X., Xia, J., Jin, C., et al. (2021). Spatial evolution of population change in Northeast China during 1992-2018. *Science of the Total Environment, 776*, 146023.
Zhao, C. (2018). Linking the Local climate zones and land surface temperature to investigate the surface urban heat island, a case study of San Antonio, Texas, U.S. *ISPRS Annals of Photogrammetry Remote Sensing and Spatial Information Sciences, IV-3*, 277–283.
Zhao, N., Ma, A., Zhong, Y., Zhao, J., & Cao, L. (2019). Self-training classification framework with spatial-contextual information for local climate zones. *Remote Sensing, 11*, 2828.
Zheng, Y., Ren, C., Xu, Y., Wang, R., Ho, J., Lau, K., et al. (2018). GIS-based mapping of local climate zone in the high-density city of Hong Kong. *Urban Climate, 24*, 419–448.
Zhou, W., Wang, J., & Cadenasso, M. L. (2017). Effects of the spatial configuration of trees on urban heat mitigation: A comparative study. *Remote Sensing of Environment, 195*, 1–12.